HHS Public Access

Author manuscript

Annu Rev Biomed Eng. Author manuscript; available in PMC 2019 June 04.

Published in final edited form as:

Annu Rev Biomed Eng. 2018 June 04; 20: 119–143. doi:10.1146/annurev-bioeng-062117-121139.

Bone Mechanical Properties in Healthy and Diseased States

Elise F. Morgan, **Ginu U. Unnikrisnan**, and **Amira I. Hussein**

Orthopaedic and Developmental Biomechanics Laboratory, Department of Mechanical Engineering, Boston University, Boston, Massachusetts 02215, USA

Abstract

The mechanical properties of bone are fundamental to the ability of our skeletons to support movement and to provide protection to our vital organs. As such, deterioration in mechanical behavior with aging and/or diseases such as osteoporosis and diabetes can have profound consequences for individuals' quality of life. This article reviews current knowledge of the basic mechanical behavior of bone at length scales ranging from hundreds of nanometers to tens of centimeters. We present the basic tenets of bone mechanics and connect them to some of the arcs of research that have brought the field to recent advances. We also discuss cortical bone, trabecular bone, and whole bones, as well as multiple aspects of material behavior, including elasticity, yield, fracture, fatigue, and damage. We describe the roles of bone quantity (e.g., density, porosity) and bone quality (e.g., cross-linking, protein composition), along with several avenues of future research.

Keywords

cortical bone; cancellous bone; trabecular bone; bone quality; multiaxial; multiscale

1. INTRODUCTION

The bones in the human skeleton must meet a diverse set of functional demands, not all of which are mechanical in nature. Yet, setting aside the biological functions of bone as an organ system or of the bone tissues that are the main constituents of whole bones, the mechanical behavior of bone is a multifaceted, broad subject relevant to studies of clinical fractures, development, adaptation, and healing and regeneration. This review provides a foundation for these areas of study by summarizing the current state of knowledge on the basic mechanical behavior of bone at length scales ranging from hundreds of nanometers to tens of centimeters. Recognizing that this article is not the first to review the mechanics of bone, we intend to present the basic tenets and to connect them to some of the arcs of research that have brought the field to recent advances. We have chosen to emphasize what is known about the effects of aging and common diseases on the mechanical properties of bone, anticipating that this review can serve the needs of researchers from many disciplines who seek to understand the age- and disease-related bases of bone fragility.

DISCLOSURE STATEMENT

The authors are not aware of any affiliations, memberships, funding, or financial holdings that might be perceived as affecting the objectivity of this review.

2. MECHANICAL PROPERTIES OF BONE TISSUE

2.1. Cortical Bone

At the scale of 1–10 mm, bone tissue can be categorized into two types: cortical bone (also known as compact bone or dense bone) and trabecular bone (also known as cancellous bone or spongy bone). The distinction between these two types of bone tissue can be made largely on the basis of porosity: Cortical bone has a porosity of 5% to 15%, whereas the porosity of trabecular bone ranges from 40% to 95%. Cortical bone is found in the diaphysis of long bones and in the form of a thin shell surrounding the trabecular compartment in the metaphyses and epiphyses. Trabecular bone is also found in the vertebrae.

2.1.1. Basic material properties—The material behavior of cortical bone is anisotropic. The strength and tensile/compressive moduli of cortical bone along the longitudinal direction (the direction aligned with the diaphyseal axis) are greater than those along the radial and circumferential directions (Table 1). Comparatively small differences in these properties have been observed in the radial versus circumferential direction, suggesting that cortical bone can be treated as a transversely isotropic material. When loaded in tension along the longitudinal direction, cortical bone exhibits a bilinear stress–strain response in which a distinct yield point separates a linearly elastic region and a region of linear hardening that ends abruptly at a fracture strain of less than 3% (Figure 1*a*).

In contrast, for compressive loading along the longitudinal direction, rapid hardening occurs after yielding, followed by softening, before failure at approximately 1.5% strain. Cortical bone specimens loaded in the transverse direction fail in a more brittle manner compared with those loaded in the longitudinal direction. Measurements of the ultimate strength of the human femoral bone under various loading modes (Table 1) show that the strength is greatest under compression in the longitudinal direction and weakest under tensile loading in the transverse direction.

2.1.2. Viscoelasticity—The effect of loading rate on strength and modulus is only moderate, as a six-order increase in the strain rate raises the modulus only by a factor of two and the strength by a factor of three (1). During normal physical activities, bone tissue is subjected to strain rates of 0.1–1.0% strain/s, and the monotonic response of cortical bone can be assumed to have only minor rate dependency. Yet, the stiffening and strengthening effects that have been observed with increasing strain rates are still clinically relevant, because strain rates during impact loading can be more than 10-fold greater than the normal physiological range. Cortical bone is more brittle at high strain rates, and loading rate also has an effect on the accumulation of damage within bone tissue (2).

2.1.3. Damage—When cortical bone is loaded past the yield point, degradation of the material properties occurs (Figure 1*b*) (3). This is the phenomenological definition of damage. Damage to cortical bone has also been defined in terms of deterioration in the tissue microstructure and/or nanostructure, collectively known as microdamage (Figure 2*a*). The presence of microdamage in bone was first reported by Frost (4) and is now recognized to be a normal consequence of physiologic loading (5).

Microdamage may appear as debonding of the proteinaceous–hydroxyapatite composite (such as debonding of hydroxyapatite aggregates and noncollagenous proteins) or as slippage of the lamellae along one another or along cement lines (6–8). Both of these microstructural events may give rise to the residual strains that are observed upon unloading after the specimen has been loaded past the yield point.

Microdamage is a possible contributor to bone fragility but also a mechanism of toughening. In vitro mechanical tests have found that microdamage is associated with a decrease in modulus (9, 10), and a weak inverse relationship between fracture toughness and microdamage density has been reported (11). Microcrack accumulation increases exponentially with age in cortical bone and is significantly higher in the bones of women versus men (12, 13). While these collective results might suggest a prominent role for microdamage in increasing fracture risk, this mechanistic link has not been established. Moreover, in vitro studies have noted that microdamage can increase resistance to crack growth (14), particularly if the damage is in the form of linear microcracks ahead of a larger crack (15).

2.1.4. Fracture and fatigue—Fracture of cortical bone can occur from repetitive, subcritical loads (fatigue failure) or from applied loads that cause local stresses exceeding the strength of the tissue. The fracture toughness of cortical bone has been quantified in terms of the critical stress intensity factor (K_c) and the critical strain energy release rate (G_c). Values of K_{IC}, the fracture toughness for so-called mode I loading (tensile loading), range between 2 and 6 MPa√m and tend to be lower for longitudinal than for transverse fracture (15, 16) and to be lower at high strain rates (17, 18).

The anisotropic nature of the fracture toughness of cortical bone is intimately linked to the toughening mechanisms that are operative in this tissue. Intrinsic toughening mechanisms, such as sliding of collagen fibrils and nucleation of micro- and nanoscale damage, are defined as those that confer resistance to microstructural disruptions ahead of the crack tip. Extrinsic toughening mechanisms, such as crack bridging and crack deflection, reduce the driving force that acts to propagate the crack. The preferential alignment of osteons in cortical bone provides effective, extrinsic toughening that is anisotropic—a crack propagating perpendicular to the osteons (transversely oriented crack) is more likely to deflect and twist than is a crack propagating parallel to the osteon (longitudinally oriented crack)—and thus can explain the anisotropy in fracture toughness (15). In the longitudinal orientation, crack bridging by uncracked ligaments (thin or planar regions of uncracked tissue that are along the crack path) appears to be the dominant toughening mechanism (Figure 3) (15). The direction dependency of the contribution of these toughening mechanisms may also explain the anisotropy in the increase in fracture toughness with crack growth (a phenomenon known as a rising R curve) (19).

Fatigue loading results in progressive degradation of mechanical properties such as fracture toughness, modulus, and strength (20, 21). Cortical bone has greater resistance to fatigue failure in compression than in tension (22) and at higher loading frequencies (23, 24). Fluorescent and radiopaque stains that label microdamage and larger cracks within the tissue

(25, 26) have enabled more in-depth study of the relationships among microcracking, microstructure, and macroscale mechanical properties.

2.1.5. Failure under multiaxial loading—Cortical bone can be subjected to multiaxial loading conditions in the body, especially during traumatic events such as a fall. Multiaxial loading can lead to more severe reductions in stiffness (27) and fatigue life (28) as compared to uniaxial loading. However, mixed-mode loading involving mode I (tension) and mode II (shear) is associated with greater fracture toughness than mode I alone (29). Given that cortical bone is anisotropic and stronger in compression than tension, isotropic and symmetric failure criteria, such as the von Mises criterion, are not capable of describing the multiaxial strength of this tissue. Therefore, more generalized failure criteria (30–32), such as those based on the Tsai–Wu criterion, have been applied to cortical bone.

2.1.6. Micro- and nanoscale properties of cortical tissue—The mechanical properties described above pertain to specimens of cortical bone whose dimensions are on the order of several millimeters or centimeters. Early research on the mechanical properties of cortical tissue at length scales less than several hundred micrometers used conventional machining techniques to isolate beams of cortical tissue. The mechanical properties of osteons were found to vary with different collagen fiber orientations and also with the mineral density and loading modes: Stiffnesses are on the order of 4 GPa for shear loading and 5–12 GPa for tensile and compressive loading (reviewed in Reference 33). So-called pull-out and push-out tests indicate that the interfacial strength of the cement line is lower than the shear strength of the osteonal lamellae (34, 35).

Subsequent research on small-scale properties of cortical tissue has used nanoindentation, micro/nanoscratch testing, and compression testing of micropillars machined via focused ion beam or femtosecond laser. Elastic moduli measured by nanoindentation are on the order of 23 GPa and 26 GPa for osteonal and interstitial lamellae, respectively, in the longitudinal direction (36, 37), and are approximately 45% lower in the transverse direction (37). Although the nanoscale moduli appear higher than those at greater length scales (Table 1), this difference may be due to the fact that most nanoindentation measurements on bone are conducted under dry conditions (38). However, compression tests on micropillars indicate that both the strength and ductility of cortical tissue are higher at the microscale versus the macroscale (39, 40). Preliminary values of fracture toughness at the microscale appear to be similar to those measured at the macroscale (41).

2.1.7. Influence of porosity and tissue composition on the mechanical properties of cortical bone—Early research on the microstructural and compositional factors that control the mechanical properties of cortical bone focused largely on porosity and mineralization. Cortical porosity is negatively correlated with Young’s modulus (42), compressive ultimate stress (43), and fracture toughness (44). Changes in porosity account for more than 75% of the variability in the strength of the cortical bone (45), and fatigue-induced microdamage located near cortical pores may be more likely to lead to fracture than that located in regions of high mineral content (46). These relationships between porosity and mechanical properties are also notable because of the rapid increases in cortical porosity that can occur (47). Although the high stiffness and strength of cortical bone compared with

those of most other biological materials are due to bone's mineral content, the normal physiological range of mineralization is not large enough to cause substantial variations in these mechanical properties (45). However, increased mineral content, such as that which can occur with long-term bisphosphonate therapy for treatment of osteoporosis, is associated with decreased fracture toughness (48).

Recent research has investigated compositional parameters collectively known as bone quality (as opposed to porosity, which measures bone quantity). Over the course of bone formation and tissue maturation, the organic matrix undergoes biochemical changes including collagen cross-linking. Cross-links formed specifically via nonenzymatic glycation have been associated with increased brittleness of the tissue (49). Techniques such as Raman spectroscopy and Fourier transform IR spectroscopy can provide high-resolution spatial mapping of parameters indicative of the ratio of carbonate to phosphate and the relative amounts of mineral, proteoglycan, lipid, water, and nonenzymatic cross-links [also known as advanced glycation end products (AGEs)] (50, 51). Raman spectroscopy may be feasible for in vivo evaluation of bone composition (52); however, a firm consensus has yet to emerge on the role of the readouts provided by Raman as indicators of bone fragility.

2.1.8. Micro- and nanomechanical modeling of cortical bone—Micro- and nanomechanical models can improve our understanding of the structure–function relationships at multiple length scales in cortical bone. At the nanoscale, models of cortical tissue have focused on the respective arrangements of, and mechanical interactions between, mineral platelets and collagen molecules or collagen fibrils (53–59). Some of these models represent a mineral-reinforced collagen matrix, in which the anisotropy is due to the mineral, and others instead represent a collagen-reinforced mineral matrix model, in which collagen is treated as the anisotropy-forming material. At a greater length scale, several hierarchical, micromechanical models have derived the mechanical properties of Haversian cortical bone (60–63). Development of techniques to measure constituent volume fractions and orientations at the nanoscale has led to considerable advances in these types of models.

2.1.9. Effects of aging and disease on the mechanical properties of cortical bone—Age-related changes in the mechanical properties of cortical bone have been attributed to increased porosity (45), hypermineralization (64), microdamage accumulation (23), increased concentration of AGEs (65), and decreased quantity of noncollagenous proteins (66). The strength of cortical bone under tension and compression declines by approximately 2% per decade beginning in the third decade of life. Tensile ultimate strain decreases by approximately 10% per decade, from a high of 5% strain at age 20–30 years to a low of less than 1% strain above age 80 years. Fracture toughness decreases approximately 4% per decade (67–69).

Common and increasingly common diseases such as osteoporosis and diabetes involve marked changes in cortical bone's mechanical behavior. The etiology of osteoporosis is such that the effects of aging on the mechanical properties of cortical bone are not readily distinguishable from those of osteoporosis. The mechanical effects of osteoporosis therapies, however, differ among the types of therapy (70, 71), and there is concern that long-term use of antiresorptive therapies can result in decreased toughness (48, 72, 73). Increasing

evidence also indicates that diabetes is associated with lower bone toughness as compared with normal cortical bone (70, 74) and that this difference may be related to heightened accumulation of AGEs in diabetic bone (75).

Less-common bone diseases have also provided insight into the origins of the mechanical behavior of cortical bone. For example, studies of osteogenesis imperfecta, a group of rare genetic disorders that affect type I collagen and are characterized by low bone toughness, indicate that fewer enzymatic cross-links, more nonenzymatic cross-links, increased porosity, and reduced fraction of lamellar bone may all work to increase tissue brittleness (76). Alteration in mineral content and in the spatial distribution of mineral, as in Paget's disease, vitamin D deficiency, and chronic kidney disease, have also been linked to deficits in stiffness or toughness, or to changes in the manner of crack propagation (19, 77).

2.2. Mechanical Behavior of Trabecular Bone

Trabecular bone—also referred to as cancellous or spongy bone—can be viewed at the apparent level (i.e., the scale at which several trabeculae and intervening pores are simultaneously observable, typically ~5–10 mm) as a highly porous material with anisotropic mechanical properties. Due to its high porosity versus that of cortical bone, the apparent-level mechanical properties of trabecular bone are determined primarily by its porosity. More minor, but still important, contributions to the apparent-level behavior come from bone-quality parameters, namely the architectural arrangement of the trabecular network and the tissue-level properties of the individual trabeculae.

2.2.1. Basic material properties—As with cortical bone, the strength of trabecular bone is greater in compression than tension, and is lowest in shear, although these differences decrease with decreasing apparent density (78). The stress–strain curve for trabecular bone does not exhibit a clear linear region or a well-defined yield point (Figure 1*c*). Nevertheless, this tissue is frequently treated as a linear elastic material, and once the modulus is calculated from a linear or polynomial curve fit (79) to the initial portion of the curve, the yield point is defined by the 0.2% offset method.

Although trabecular bone yields at strains of approximately 0.7% in compression, it can sustain compressive strains of up to 50% while still maintaining a large fraction of its load-bearing capacity. If a specimen is compressed beyond yield (not exceeding 5% strain), unloaded, and reloaded, permanent residual strains and a loss of stiffness (as quantified by a comparison of the slope of the unloading curve to the initial elastic modulus) and strength occur (Figure 1*d*) (80). These effects occur in trabecular samples and in the entire vertebral body (81), indicating that isolated overloads that do not cause overt fracture of the bone may cause subtle but cumulative permanent deformations that could lead to clinical fractures. The qualitative similarity between this damage–reload of trabecular bone and the behavior of cortical bone loaded in tension (3) suggests that the dominant physical mechanisms underlying the damage behavior act at the nanometer scale.

2.2.2. Heterogeneity in mechanical properties due to density and architecture —Several different measures of density are used in biomechanical studies of trabecular bone. Ash density is defined as the ratio of ash weight per unit bone volume. Tissue density

is defined as the ratio of mass to volume of the mineralized tissue (i.e., the pore space is excluded from the volume calculation). Tissue density is approximately 2.0 g/cm^3 for cortical and trabecular bone and varies very little in the adult skeleton. Apparent density is the ratio of the mass of bone tissue to the total volume of the bone. Volume fraction is the ratio of the volume of the mineralized tissue to the volume of the specimen or, equivalently, one minus the porosity. The volume fraction of trabecular bone varies from 60% in primary compressive group of femoral neck to less than 10% in the elderly spine (82).

The spatial arrangement of trabeculae is known as the trabecular architecture. Quantitative measures of trabecular architecture are now routine to compute as the availability of high-resolution, three-dimensional imaging techniques such as micro–computed tomography (μCT), peripheral quantitative computed tomography (peripheral QCT), and micro–magnetic resonance imaging has increased. Measures of trabecular architecture include trabecular thickness, trabecular spacing, trabecular number, connectivity density, structure model index (SMI; a measure of how rod-like versus plate-like the architecture is), and the degree of anisotropy (83). The last of these is a scalar measure of how preferentially the trabecular structure is oriented. The most common method of quantifying the anisotropy of the trabecular structure is by using the mean intercept length (MIL) (84). MIL, as well as other methods, quantifies the directional density (the amount of tissue in a given direction) of the tissue. The data on directional density for a given specimen or region can be represented graphically by an ellipsoid, for which the ratio of the major and minor axes is the degree of anisotropy, and analytically by the fabric tensor, a positive definite, second-order tensor whose eigenvalues are the lengths of the major, minor, and intermediate axes of the ellipsoid (85, 86).

Trabecular bone can display substantial spatial heterogeneity in both density and architecture, even within a given anatomic site. For example, in the vertebrae, variations in density and architecture have been observed along the superior–inferior and posterior–anterior directions (87). Young’s modulus can vary by as much as 100-fold, and strength as much as fivefold, within a single epiphysis (88). These variations in density and architecture can then lead to heterogeneity in the apparent-level elastic and strength properties of trabecular bone. Typically, the modulus of human trabecular bone ranges between 10 and 3,000 MPa, whereas strength, which is linearly and strongly correlated with modulus (82, 89), is generally two orders of magnitude smaller, in the range 0.1–30 MPa. Approximately 70–90% of the variances in the modulus and strength of trabecular bone can be explained by volume fraction or apparent density (90, 91). These dependencies are typically described using linear or power-law relationships. Numerous studies have indicated that the power-law exponent for human trabecular bone is between two and three for modulus (91) and two for compressive strength (Figure 4) (82). That these exponents are greater than one suggests that small decreases in density that occur in the course of the normal aging process have severe consequences for the load-bearing capacity of trabecular bone. However, often these power-law relations are obtained from sets of bone specimens that collectively span a wide range of densities and are pooled from multiple sites. Within a single anatomic site, the modulus and strength relations appear to be linear because the range of apparent density is less than an order of magnitude (82, 91).

The anisotropy that trabecular bone exhibits in microstructure is also present in elastic modulus (89) and strength (92). Indeed, the principal directions of the mechanical anisotropy of trabecular bone are very closely aligned with the principal directions (eigenvectors) of the fabric tensor (93). Trabecular bone often exhibits orthotropic symmetry (94, 95), although in some cases, such as in the vertebrae, transverse isotropy has been reported (93). Note, however, that in regions of the vertebrae with low volume fraction, the trabecular network may be too sparse and spatially heterogeneous to allow proper definition of the type of anisotropy and the material properties (96).

2.2.3. Yield strain—Yield strain is a notable exception to the above-mentioned mechanical anisotropy and density dependence of trabecular bone. High-density trabecular bone, such as that from the human femoral neck and bovine proximal tibia, tends to have isotropic yield strains (97, 98). The compressive yield strains of human vertebral trabecular bone, which is of much lower density, are higher when the loading direction is 45° oblique to the principal direction as compared to when the loading is on-axis, but the difference is less than 10% (98). Ultimate strains in trabecular bone also appear to be isotropic and range from 1.0% to 2.5% (97, 99), whereas yield strains range from 0.70% to 0.77% in compression and from 0.65% to 0.71% in tension (82).

Yield strains in trabecular bone exhibit only a weak dependence on apparent density and volume fraction (82). Compressive yield strains increase slightly with increasing density for human vertebral trabecular bone and are not dependent on density for higher-density trabecular bone. Overall, standard deviations of yield strains within a given anatomic site are on the order of one-tenth of the mean, whereas significant differences in the means tend to occur between sites, indicating that yield strains can be considered relatively constant within sites but different among sites (82). Thus, characterizing yield in trabecular bone in terms of strain rather than stress can provide a greatly simplified picture of failure in this tissue, because a strain-based failure criterion may not need to account for interspecimen differences in apparent density.

2.2.4. Viscoelasticity—The compressive modulus and compressive strength are proportional to the strain rate raised to the power of 0.06 (100, 101). Both stress- and strain-dependent effects in stress–relaxation experiments have been observed (102), indicating that trabecular bone is technically nonlinearly viscoelastic. Trabecular bone has similar creep characteristics as cortical bone and exhibits an initial rapid increase in strain followed by a steady-state regime with a constant creep rate and, finally, another rapid increase in strain just prior to creep fracture (103).

2.2.5. Damage—The large reduction in apparent modulus that occurs with overloading (Figure 2*b*) results from damage within the trabeculae, namely microscopic cracking as opposed to overt fracture of individual trabeculae (104). The occurrence of microdamage appears to be related to the magnitudes of both apparent- and tissue-level strains (105–107). Measurements of tissue-level deformations via digital image correlation applied to bending tests of single trabeculae indicate that microdamage initiation occurs at tissue-level strains of approximately 1.6% and differs in compression versus tension (108); however, estimates from finite element (FE) models suggest that the threshold for damage initiation is lower

(107). It is important to consider that, due to the porous, irregular structure of trabecular bone, some tissue-level strains can be high enough to induce local yielding and a concomitant decline in whole-specimen properties even for low magnitudes of apparent stress (106, 109), consistent with the idea that the presence of microdamage in vivo in trabecular tissue is the norm, not the exception.

In general, microdamage increases with age, similar to the case with cortical bone, and under both pre- and postyield loading conditions, the occurrence of microdamage is correlated with architectural parameters and volume fraction. For example, more microdamage is found in regions with low volume fraction and high SMI—indicating a predominance of trabecular rods (110, 111). The propagation of damage and yielding in trabecular bone is also anisotropic in a manner that relates to the orientation and local thickness of the trabeculae (112).

2.2.6. Fracture and fatigue—The fracture toughness of trabecular bone has not been studied extensively, because the porous and spatially heterogeneous microstructure presents a significant challenge for meeting the requirements of a fracture-toughness test. Fracture toughness does appear to append on density (113).

Cyclic compressive loading of trabecular bone can cause loss of stiffness and strength as well as the accumulation of residual strain even for low levels of applied load (114, 115). The rates at which modulus decreases and damage accumulation occurs in fatigue increase with increasing magnitudes of applied strain (114). The mechanisms of failure in fatigue appear to occur at the nanoscale (116). Static and cyclic tests on human trabecular specimens under physiologic loads (750–1,500 microstrain) indicate that the time required for full recovery of residual deformation is more than 20 times longer than the duration of the applied loads (115). These results support the idea that nontraumatic fractures may be related to long-term creep effects, whether accumulated during long-term static loading or fatigue loading.

The compressive fatigue life of trabecular bone is also a function of fabric. The number of cycles to failure in human vertebral trabecular bone is well predicted by a power-law relationship in which the independent variables are volume fraction, fabric, and applied stress, and a significant contribution of the degree of anisotropy toward the prediction of fatigue life has been observed (117). The latter result is consistent with the finding that fatigue life is lower for loading oblique to the principal direction (off-axis) versus along the principal direction (on-axis) (118).

2.2.7. Yield and failure under multiaxial loading—Because complex loading conditions can exist in vivo and nonhabitual events such as falls or accidents can induce off-axis loads, a multiaxial failure criterion for trabecular bone is needed. Early theoretical research on multiaxial failure in trabecular proposed fabric-based yield criteria (119, 120). These criteria were not experimentally validated at the time, because some of the necessary data, such as the tensile and compressive strengths of a given specimen, were not obtainable through experiments. This barrier was subsequently overcome using numerical simulation, as discussed in Section 2.2.9, below, and there now exist several multiaxial yield criteria for

trabecular bone (see References 121–123 and references therein). As several of these studies have found, casting the yield criterion in terms of strain, rather than stress, eliminates nearly all of the dependence of the yield surface on porosity and much of its dependence on fabric. At present, there is no consensus on which criterion is most accurate for trabecular bone, largely because none has been validated using an independent set of specimens. Further research is also needed to build on recent advances in studying the multiaxial mechanical behavior of trabecular bone following yield (124, 125).

2.2.8. Analytical modeling—Seminal research in the development of analytical models for the mechanical behavior of trabecular bone considered this porous tissue a cellular solid (126). Using this approach, investigators attributed the experimentally observed dependence of Young's modulus and compressive strength on apparent density raised to the second power to bending-dominated linear elastic behavior and failure by buckling (127).

Other analytical models incorporate less-idealized descriptions of trabecular architecture via use of the fabric tensor. Cowin (86) developed equations for relating the elastic constants of an orthotropic material to its porosity and fabric. These relations were further developed to uncouple volume fraction from fabric (128) and to ensure positive definiteness of the elasticity tensor a priori (129). More recent research has indicated that the fabric–mechanical property relationships may depend on anatomic site (130). The development of these analytical models for the prediction of apparent-level elastic properties from morphological parameters of trabecular bone contributes to the ability to evaluate disease progression and bone stiffness noninvasively in a clinical setting, in addition to providing a foundation for the development of numerical models.

2.2.9. Numerical modeling—The advantages of analytical models in providing closed-form relationships for the mechanical properties of trabecular bone must be balanced against the errors in the model predictions that arise from oversimplifications of the trabecular architecture and tissue-level material properties. Numerical models that more closely approximate the irregularity of the trabecular architecture and the inhomogeneity in both architecture and tissue-level properties have been employed (e.g., 131). In parallel, so-called micro-FE models, which are FE models built directly from μCT scans of trabecular bone (132), have become a standard tool in the study of trabecular bone mechanics. In these models, the individual trabeculae within the specimen are resolved with the same, or nearly the same, level of anatomic detail as the μCT images themselves.

To date, micro-FE analyses of trabecular bone have been used in two general areas of study. The first complements the use of analytical models to elucidate structure–function relationships for the elastic and yield behavior at the apparent level. For this area, the ability to test each specimen multiple times—that is, along different loading directions or in different loading modes—is of great benefit. For example, Kabel et al. (133) used micro-FE analysis to estimate all nine orthotropic elastic constants of specimens of trabecular bone from multiple anatomic sites and employed these data to determine the values of the coefficients in the fabric–elasticity relationships proposed earlier by Cowin (86). These results confirmed the primary role of both volume fraction and microstructural anisotropy in determining apparent elastic properties. Combination of the micro-FE approach with digital

topological analysis (134), a method of classifying the individual trabeculae within a specimen as rods or plates and of quantifying the orientation of each trabecula, has enabled study of the way in which trabecular architecture, and changes in architecture, transmits force and confers bone stiffness and strength. In doing so, this combined approach has provided a direct bridge between the mechanistic approach of cellular-solid modeling and the anatomic fidelity of micro-FE analysis.

The second area of study involves the use of micro-FE modeling to estimate distributions of stress and strain within trabecular tissue in response to loads applied either at the apparent level or to the whole bone. These distributions have been correlated with microdamage accumulation (105), bone formation/resorption (135), and bone failure (112).

2.2.10. Mechanical properties of trabecular tissue—Trabecular tissue, which is the bony tissue that comprises individual trabeculae, is similar to cortical bone in both composition and material properties. Tensile tests (136), ultrasonic measurements (137), nanoindentation (138), and scanning acoustic microscopy (139) techniques indicate that the elastic modulus of trabecular tissue is around 10–20 GPa. Recent research indicates that the mechanical properties of trabecular tissue, especially the ultimate strain and toughness, are correlated Raman spectroscopic readouts such as collagen cross-linking (140).

Elastic and strength properties have also been reported using a combined FE analytical–experimental approach. In these studies, the tissue modulus is determined from a ratio to apparent modulus calibrated against experimental results (141). Results from this approach place the elastic modulus of human trabecular tissue at approximately 10% less, tensile yield strain at 15% less, and tensile/compressive tissue strength at 25% less than that of cortical bone (142). This ranking is consistent with the results of a comparison of measured fatigue strengths in trabecular versus cortical tissue (143). However, despite the poorer mechanical performance of trabecular tissue compared with that of cortical tissue, several groups of investigators have noted that trabeculae can sustain large bending deformations without catastrophic loss of load-carrying capacity (136, 144).

2.2.11. Effects of aging and disease on the mechanical behavior of trabecular bone—The density and architecture of trabecular bone undergo profound changes with age. The trabeculae become progressively thinner and less closely spaced; the overall structure exhibits a large decrease in connectivity and volume fraction. For certain anatomic sites, such as the vertebral body and proximal tibia, an increase in the anisotropy of the trabecular structure is observed (Figure 5) (145, 146).

Both modulus and strength decrease with age, falling by approximately 10% per decade (92, 147). Due to the coupling between age-related changes in density and architecture, much of the age-related decrease in stiffness and strength can be explained by the changes in density. However, the magnitude of the anisotropy in compressive strength appears to increase with age (92), consistent with the increase in the degree of anisotropy of the trabecular structure. Pronounced changes in trabecular architecture have also been observed in osteoarthritis (148), and evidence suggests that the relatively sclerotic appearance of the osteoarthritic trabecular structure may coexist with lower mineral density and stiffness of the tissue (149).

Few data are available on whether aging or disease affect trabecular tissue differently than cortical tissue. As such, it is not yet clear whether differences in the age- or disease-related mechanical properties of trabecular bone would be expected beyond the differences predicted by the changes in volume fraction and architecture of the trabecular bone and the changes in mechanical properties of cortical bone.

3. MECHANCIAL BEHAVIOR OF WHOLE BONES

Thus far, our discussion of the mechanical properties of bone has focused on the properties of trabecular and cortical bone as separate tissues, and as determined from mechanical tests performed on excised specimens of these tissues. How these two different tissues combine to form a whole bone, such as the femur, dictates the overall mechanical behavior of that bone. In addition to the respective amounts of cortical and trabecular bone that are present, structural and geometric features, such as cortical thickness, the spatial distribution of trabecular bone, cross-sectional area, bone size, and bone shape, all influence whole-bone mechanical properties, and all change with age and disease. The study of the mechanical behavior of whole bones can thus be substantially more complicated than the study of cortical or trabecular bone. However, investigations at the whole-bone level are arguably the ones most directly relevant to understanding the occurrence of fractures, the biomechanics of healing of those fractures, and both the mechanical input for and the outcomes of bone adaptation. Moreover, for rodent models in bone mechanics, whole-bone tests are one of the most practical options for mechanical investigations, given the small size of the skeleton. Indeed, isolation of an apparent-level specimen of trabecular bone is not possible in most cases, due to the small amounts of this tissue in any given anatomic site.

3.1. Loading of Whole Bones In Vivo and In Vitro

A major challenge in the design of laboratory tests that seek to characterize clinically relevant mechanical behavior of a whole bone is to identify loading conditions that are physiologically representative. These loading conditions have been estimated using gait analysis, instrumented prostheses, and in some cases, direct measurement in tissues. Despite many advances in these techniques, however, biological variation and other uncertainties associated with measuring joint contact forces, muscle forces, and impact conditions in vivo still hinder accurate and precise estimates of the directions, magnitudes, and locations of the forces and moments that should be applied ex vivo. Moreover, in vivo loading conditions can be sufficiently complex, involving multiple muscle groups and distributed loads across a joint surface, to present major difficulties in recapitulating them ex vivo. Nevertheless, using simplified loading conditions, many ex vivo experiments produce fracture patterns commonly observed in the clinical setting.

3.2. Role of Geometry in Whole-Bone Mechanical Behavior

Principles of engineering mechanics stipulate that the axial stiffness, in either compression or tension, of a structure is proportional to the cross-sectional area, while the bending and torsional stiffnesses of beam-like structures (such as diaphyses) depend on how the material (tissue) is distributed around the axis of bending or twist. Two geometric properties, the areal moment of inertia (also known as the cross-sectional moment of inertia) and the polar

moment of inertia, quantify this distribution in manners relevant for bending and torsion, respectively.

These two geometric properties, when multiplied by the relevant elastic modulus (Young's modulus in the case of axial loading and bending, and shear modulus in the case of torsion), constitute a measure of structural rigidity. Given that the moduli are heterogeneous throughout a whole bone, one approach for estimating the structural rigidity is to use the spatial variations in local intensities within a computed tomography image of the cross section as estimates of the spatial variations in tissue mineral density and then use density–modulus relationships to avoid the assumption of a homogeneous modulus distribution (150). This method has provided estimates of structural rigidity that are correlated with the strength and stiffness of vertebrae with metastases or simulated lytic lesions, but it appears to be less effective for the comparatively subtle changes in vertebral trabecular bone due to aging (151).

Conversely, if one has measured the stiffness or rigidity of a whole bone, some estimates of the material properties of the bone tissue can be derived. If the bone is straight, prismatic (i.e., the cross-sectional geometry does not change along the length of the structure), and of uniform composition, it is straightforward to calculate Young's modulus or shear modulus from the value of stiffness obtained from the whole-bone test. However, none of these three descriptors are accurate for vertebral bodies, metaphyses, and diaphyses due to the irregular geometry and spatially heterogeneous composition of these bones. For diaphyses, one can calculate an effective elastic modulus of the tissue if the true cross-sectional geometry and its variation along the diaphyseal axis are included in the calculations. Without accounting for the true geometry, substantial errors in the calculated modulus can result (152).

3.3. Effect of Aging and Disease on the Mechanical Behavior of Whole Bones

Cross-sectional geometry and other geometric features of whole bones exhibit marked changes with age. The general pattern of age-related change in the cross-sectional geometry of the diaphysis is continual apposition of bone at the periosteal surface, accompanied by resorption of bone at the endosteal surface. The net result is a thinner cortex and smaller cross-sectional area (despite the increase in periosteal diameter), but not necessarily any decrease in the moments of inertia (Figure 6) (153). The relatively small changes in moment of inertia with age serve to ameliorate the structural consequences of the age-related decline in the amount of bone present, although some controversy exists as to the magnitude of, and gender differences in, this benefit (154). Experimental and numerical studies have indicated that the strength of the proximal femur declines by approximately 10–12% per decade of life, or by approximately 50% from early to late adulthood (155–157).

For the vertebrae, an increase in the cross-sectional area with aging has been reported for both men and women (154), and one study found that this increase was three times greater in men than in women (158). Thus, in a manner similar to the diaphysis but in an anatomic site that has a large fraction of trabecular bone, age-related bone loss in the vertebral centrum is accompanied by an increase in the surface area carrying the load. At the same time, age-related bone loss occurs nonuniformly throughout the vertebrae in a manner that differs between men and women (159); as such, the effect of the age-related increase in cross-

sectional area is difficult to isolate. As estimated from FE analyses based on QCT scans, vertebral strength declines with age more quickly in women than in men, and more quickly in the lumbar versus thoracic spine (160), despite the roughly equal proportion of fractures in these two regions.

Differences in bone geometry have also been found between individuals with and without osteoporotic fractures. For the proximal femur, neck-shaft angle and bone diameter are larger in individuals with fracture compared with those of control subjects (161). Whether these differences are causal is not clear, although differences in the neck-shaft angle can affect the magnitude of the stresses and strains that the femoral neck experiences under both gait and fall conditions. Regarding the axial skeleton, a comparison between fracture and nonfracture cohorts found that the vertebral cross-sectional area was lower in the former (158). Other geometric features of the vertebra, such as shell curvature and end-plate curvature, may also play a role (162–164).

Not all fragility fractures can be attributed to osteoporosis (at least as defined by low bone density), and evidence from studies of bone mechanics in individuals with diabetes suggests that a combination of geometric and material properties play a role. In postmenopausal women with type 2 diabetes, cortical porosity is elevated in individuals with a history of fragility fractures compared with nonfracture controls (165). However, an association between cortical porosity and diabetes may depend on anatomic site (166), and not all measures of bone microstructure are deficient in diabetics versus controls (167). Data from rodent models of diabetes support the idea that, in diabetes, poorer whole-bone performance can be attributed to deleterious changes in the mechanical behavior of bone tissue, beyond any changes in bone geometry (74).

4. CONCLUDING REMARKS

Aging and disease can cause substantial changes in the mechanical properties of cortical bone, trabecular bone, and whole bones. Although porosity is the physical property most responsible for, or at least most closely associated with, many of these age- and disease-related changes, the arc of research on the mechanical behavior of bone has drawn in a multitude of bone-quality parameters that can be consequential as well. In parallel with the push to use measurements of bone quality and quantity to improve predictions of increased bone fragility with age and common diseases, recent research has expanded further into mechanical characterization of bone tissue at the nanoscale. This research has deepened our understanding of the intricate interactions among the chemical composition, nanostructure, and mechanical performance of cortical and trabecular bone.

Although these advances at small length scales may be far from influencing clinical predictions of fracture risk, they are important for establishing mechanisms by which specific aspects of bone biology control bone’s mechanical performance. As these insights are integrated into models and measurements of the mechanical behavior—in particular the yield, postyield, and fracture behavior—of bone at larger length scales, ultimately to the level of the whole bone, they are likely to enable new and more personalized treatments to

mitigate the negative consequences of aging and disease on the mechanical competence of bone.

Acknowledgments

The writing of this review was supported in part by grants from the National Science Foundation (CMMI 6775754, CMMI 1266243) and the National Institutes of Health (AR054620).

LITERATURE CITED

1. McElhaney JH. Dynamic response of bone and muscle tissue. J Appl Physiol. 1966; 21:1231–36. [PubMed: 5916656]
2. Zioupos P, Hansen U, Currey JD. Microcracking damage and the fracture process in relation to strain rate in human cortical bone tensile failure. J Biomech. 2008; 41:2932–39. [PubMed: 18786670]
3. Fondrk MT, Bahniuk EH, Davy DT. A damage model for nonlinear tensile behavior of cortical bone. J Biomech Eng. 1999; 121:533–41. [PubMed: 10529922]
4. Frost HM. Presence of microscopic cracks in vivo in bone. Henry Ford Hosp Bull. 1960; 8:27–35.
5. Martin RB. Fatigue microdamage as an essential element of bone mechanics and biology. Calcif Tissue Int. 2003; 73:101–7. [PubMed: 14565590]
6. Varvani-Farahani A, Najmi H. A damage assessment model for cadaveric cortical bone subjected to fatigue cycles. Int J Fatigue. 2010; 32:420–27.
7. Poundarik AA, Diab T, Sroga GE, Ural A, Boskey AL, et al. Dilatational band formation in bone. PNAS. 2012; 109:19178–83. [PubMed: 23129653]
8. Jepsen KJ, Davy DT, Krzypow DJ. The role of the lamellar interface during torsional yielding of human cortical bone. J Biomech. 1999; 32:303–10. [PubMed: 10093030]
9. Burr DB, Turner CH, Naick P, Forwood MR, Ambrosius W, et al. Does microdamage accumulation affect the mechanical properties of bone? J Biomech. 1998; 31:337–45. [PubMed: 9672087]
10. Nicolella DP, Ni Q, Chan KS. Non-destructive characterization of microdamage in cortical bone using low field pulsed NMR. J Mech Behav Biomed Mater. 2011; 4:383–91. [PubMed: 21316626]
11. Norman TL, Yeni YN, Brown CU, Wang Z. Influence of microdamage on fracture toughness of the human femur and tibia. Bone. 1998; 23:303–6. [PubMed: 9737354]
12. Courtney AC, Hayes WC, Gibson LJ. Age-related differences in post-yield damage in human cortical bone. Experiment and model. J Biomech. 1996; 29:1463–71. [PubMed: 8894927]
13. Schaffler MB, Radin EL, Burr DB. Mechanical and morphological effects of strain rate on fatigue of compact bone. Bone. 1989; 10:207–14. [PubMed: 2803855]
14. Vashishth D, Tanner KE, Bonfield W. Contribution, development and morphology of micro-cracking in cortical bone during crack propagation. J Biomech. 2000; 33:1169–74. [PubMed: 10854892]
15. Nalla RK, Stolken JS, Kinney JH, Ritchie RO. Fracture in human cortical bone: local fracture criteria and toughening mechanisms. J Biomech. 2005; 38:1517–25. [PubMed: 15922763]
16. Bonfield W, Datta PK. Fracture toughness of compact bone. J Biomech. 1976; 9:131–34. [PubMed: 1254608]
17. Zimmermann EA, Gludovatz B, Schaible E, Busse B, Ritchie RO. Fracture resistance of human cortical bone across multiple length scales at physiological strain rates. Biomaterials. 2014; 35:5472–81. [PubMed: 24731707]
18. Gauthier R, Follet H, Langer M, Meille S, Chevalier J, et al. Strain rate influence on human cortical bone toughness: a comparative study of four paired anatomical sites. J Mech Behav Biomed Mater. 2017; 71:223–30. [PubMed: 28360020]
19. Zimmermann EA, Busse B, Ritchie RO. The fracture mechanics of human bone: influence of disease and treatment. BoneKEy Rep. 2015; 4:743. [PubMed: 26380080]
20. Pattin CA, Caler WE, Carter DR. Cyclic mechanical property degradation during fatigue loading of cortical bone. J Biomech. 1996; 29:69–79. [PubMed: 8839019]

21. Fletcher L, Codrington J, Parkinson I. Effects of fatigue induced damage on the longitudinal fracture resistance of cortical bone. J Mater Sci Mater Med. 2014; 25:1661–70. [PubMed: 24715332]
22. Carter DR, Hayes WC. Compact bone fatigue damage—I. Residual strength and stiffness. J Biomech. 1977; 10:325–37. [PubMed: 893471]
23. Zioupos P, Currey JD, Casinos A. Tensile fatigue in bone: Are cycles-, or time to failure, or both, important? J Theor Biol. 2001; 210:389–99. [PubMed: 11397140]
24. Caler WE, Carter DR. Bone creep–fatigue damage accumulation. J Biomech. 1989; 22:625–35. [PubMed: 2808445]
25. Lee TC, Arthur TL, Gibson LJ, Hayes WC. Sequential labelling of microdamage in bone using chelating agents. J Orthop Res. 2000; 18:322–25. [PubMed: 10815835]
26. Landrigan MD, Li J, Turnbull TL, Burr DB, Niebur GL, Roeder RK. Contrast-enhanced microcomputed tomography of fatigue microdamage accumulation in human cortical bone. Bone. 2011; 48:443–50. [PubMed: 20951850]
27. Zysset PK, Curnier A. A 3D damage model for trabecular bone based on fabric tensors. J Biomech. 1996; 29:1549–58. [PubMed: 8945653]
28. George WT, Vashishth D. Susceptibility of aging human bone to mixed-mode fracture increases bone fragility. Bone. 2006; 38:105–11. [PubMed: 16182625]
29. Olvera D, Zimmermann EA, Ritchie RO. Mixed-mode toughness of human cortical bone containing a longitudinal crack in far-field compression. Bone. 2012; 50:331–36. [PubMed: 22115793]
30. Cezayirlioglu H, Bahniuk E, Davy DT, Heiple KG. Anisotropic yield behavior of bone under combined axial force and torque. J Biomech. 1985; 18:61–69. [PubMed: 3980489]
31. Schwiedrzik JJ, Wolfram U, Zysset PK. A generalized anisotropic quadric yield criterion and its application to bone tissue at multiple length scales. Biomech Model Mechanobiol. 2013; 12:1155–68. [PubMed: 23412886]
32. Arramon YP, Mehrabadi MM, Martin DW, Cowin SC. A multidimensional anisotropic strength criterion based on Kelvin modes. Int J Solids Struct. 2000; 37:2915–35.
33. Ascenzi A, Baschieri P, Benvenuti A. The torsional properties of single selected osteons. J Biomech. 1994; 27:875–84. [PubMed: 8063838]
34. Dong XN, Zhang X, Guo XE. Interfacial strength of cement lines in human cortical bones. Mech Chem Biosyst. 2005; 2:63–68. [PubMed: 16783927]
35. Bigley RF, Griffin LV, Christensen L, Vandenbosch R. Osteon interfacial strength and histomorphometry of equine cortical bone. J Biomech. 2006; 39:1629–40. [PubMed: 16019009]
36. Rho J-Y, Tsui TY, Pharr GM. Elastic properties of human cortical and trabecular lamellar bone measured by nanoindentation. Biomaterials. 1997; 18:1325–30. [PubMed: 9363331]
37. Franzoso G, Zysset PK. Elastic anisotropy of human cortical bone secondary osteons measured by nanoindentation. J Biomech Eng. 2009; 131:021001. [PubMed: 19102560]
38. Hoffler CE, Guo XE, Zysset PK, Goldstein SA. An application of nanoindentation technique to measure bone tissue lamellae properties. J Biomech Eng. 2005; 127:1046–53. [PubMed: 16502646]
39. Schwiedrzik J, Raghavan R, Burki A, LeNader V, Wolfram U, et al. In situ micropillar compression reveals superior strength and ductility but an absence of damage in lamellar bone. Nat Mater. 2014; 13:740–47. [PubMed: 24907926]
40. Tertuliano OA, Greer JR. The nanocomposite nature of bone drives its strength and damage resistance. Nat Mater. 2016; 15:1195–202. [PubMed: 27500809]
41. Kataruka A, Mendu K, Okeoghene O, Puthuvelil J, Akono AT. Microscopic assessment of bone toughness using scratch tests. Bone Rep. 2017; 6:17–25. [PubMed: 28377977]
42. Schaffler MB, Burr DB. Stiffness of compact bone: effects of porosity and density. J Biomech. 1988; 21:13–16. [PubMed: 3339022]
43. Behrens JC, Walker PS, Shoji H. Variations in strength and structure of cancellous bone at the knee. J Biomech. 1974; 7:201–7. [PubMed: 4844327]

44. Ural A, Vashishth D. Effects of intracortical porosity on fracture toughness in aging human bone: a microCT-based cohesive finite element study. J Biomech Eng. 2007; 129:625–31. [PubMed: 17887887]
45. McCalden RW, McGeough JA, Barker MB, Court-Brown CM. Age-related changes in the tensile properties of cortical bone: the relative importance of changes in porosity, mineralization and microstructure. J Bone Joint Surg. 1993; 75:A1193–205.
46. Turnbull TL, Baumann AP, Roeder RK. Fatigue microcracks that initiate fracture are located near elevated intracortical porosity but not elevated mineralization. J Biomech. 2014; 47:3135–42. [PubMed: 25065731]
47. Kovacs CS. The skeleton is a storehouse of mineral that is plundered during lactation and (fully?) replenished afterwards. J Bone Miner Res. 2017; 32:676–80. [PubMed: 28177150]
48. Lloyd AA, Gludovatz B, Riedel C, Luengo EA, Saiyed R, et al. Atypical fracture with long-term bisphosphonate therapy is associated with altered cortical composition and reduced fracture resistance. PNAS. 2017; 114:8722–27. [PubMed: 28760963]
49. Vashishth D, Gibson GJ, Khoury JI, Schaffler MB, Kimura J, Fyhrie DP. Influence of nonenzymatic glycation on biomechanical properties of cortical bone. Bone. 2001; 28:195–201. [PubMed: 11182378]
50. Boskey AL. Bone composition: relationship to bone fragility and antiosteoporotic drug effects. BoneKEy Rep. 2013; 2:447. [PubMed: 24501681]
51. Mandair GS, Morris MD. Contributions of Raman spectroscopy to the understanding of bone strength. BoneKEy Rep. 2015; 4:620. [PubMed: 25628882]
52. Buckley K, Kerns JG, Vinton J, Gikas PD, Smith C, et al. Towards the in vivo prediction of fragility fractures with Raman spectroscopy. J Raman Spectrosc. 2015; 46:610–18. [PubMed: 27546955]
53. Jager I, Fratzl P. Mineralized collagen fibrils: a mechanical model with a staggered arrangement of mineral particles. Biophys J. 2000; 79:1737–46. [PubMed: 11023882]
54. Yuan F, Stock SR, Haeffner DR, Almer JD, Dunand DC, Brinson LC. A new model to simulate the elastic properties of mineralized collagen fibril. Biomech Model Mechanobiol. 2011; 10:147–60. [PubMed: 20521160]
55. Nair AK, Gautieri A, Buehler MJ. Role of intrafibrillar collagen mineralization in defining the compressive properties of nascent bone. Biomacromolecules. 2014; 15:2494–500. [PubMed: 24892376]
56. Abueidda DW, Sabet FA, Jasiuk IM. Modeling of stiffness and strength of bone at nanoscale. J Biomech Eng. 2017; 139:051006.
57. Pidaparti RMV, Chandran A, Takano Y, Turner CH. Bone mineral lies mainly outside collagen fibrils: predictions of a composite model for osternal bone. J Biomech. 1996; 29:909–16. [PubMed: 8809621]
58. Katz JL. Anisotropy of Young's modulus of bone. Nature. 1980; 283:106–7. [PubMed: 7350519]
59. Hellmich C, Barthelemy J, Dormieux L. Mineral-collagen interactions in elasticity of bone ultrastructure—a continuum micromechanics approach. Eur J Mech A. 2004; 23:783–810.
60. Deuerling JM, Yue W, Espinoza Orias AA, Roeder RK. Specimen-specific multi-scale model for the anisotropic elastic constants of human cortical bone. J Biomech. 2009; 42:2061–67. [PubMed: 19664772]
61. Yoon YJ, Cowin SC. The estimated elastic constants for a single bone osteonal lamella. Biomech Model Mechanobiol. 2008; 7:1–11. [PubMed: 17297631]
62. Sansalone V, Naili S, Bousson V, Bergot C, Peyrin F, et al. Determination of the heterogeneous anisotropic elastic properties of human femoral bone: from nanoscopic to organ scale. J Biomech. 2010; 43:1857–63. [PubMed: 20392446]
63. Martínez-Reina J, Domínguez J, García-Aznar J. Effect of porosity and mineral content on the elastic constants of cortical bone: a multiscale approach. Biomech Model Mechanobiol. 2010; 10:309–22. [PubMed: 20596743]
64. Currey JD, Brear K, Zioupos P. The effects of ageing and changes in mineral content in degrading the toughness of human femora. J Biomech. 1996; 29:257–60. [PubMed: 8849821]

65. Wang X, Shen X, Li X, Mauli Agrawal C. Age-related changes in the collagen network and toughness of bone. Bone. 2002; 31:1–7. [PubMed: 12110404]
66. Sroga GE, Vashishth D. Effects of bone matrix proteins on fracture and fragility in osteoporosis. Curr Osteoporos Rep. 2012; 10:141–50. [PubMed: 22535528]
67. Nalla RK, Kruzic JJ, Kinney JH, Ritchie RO. Effect of aging on the toughness of human cortical bone: evaluation by R-curves. Bone. 2004; 35:1240–46. [PubMed: 15589205]
68. Burstein A, Reilly D, Martens M. Aging of bone tissue: mechanical properties. J Bone Joint Surg Am. 1976; 58:82–86. [PubMed: 1249116]
69. Koester KJ, Barth HD, Ritchie RO. Effect of aging on the transverse toughness of human cortical bone: evaluation by R-curves. J Mech Behav Biomed Mater. 2011; 4:1504–13. [PubMed: 21783160]
70. Campbell GM, Tiwari S, Picke AK, Hofbauer C, Rauner M, et al. Effects of insulin therapy on porosity, non-enzymatic glycation and mechanical competence in the bone of rats with type 2 diabetes mellitus. Bone. 2016; 91:186–93. [PubMed: 27497735]
71. Brock GR, Chen JT, Ingraffea AR, MacLeay J, Pluhar GE, et al. The effect of osteoporosis treatments on fatigue properties of cortical bone tissue. Bone Rep. 2015; 2:8–13. [PubMed: 25642445]
72. Allen MR, Burr DB. Bisphosphonate effects on bone turnover, microdamage, and mechanical properties: what we think we know and what we know that we don't know. Bone. 2011; 49:56–65. [PubMed: 20955825]
73. Chapurlat RD, Delmas PD. Bone microdamage: a clinical perspective. Osteoporos Int. 2009; 20:1299–308. [PubMed: 19291343]
74. Nyman JS, Even JL, Jo CH, Herbert EG, Murry MR, et al. Increasing duration of type 1 diabetes perturbs the strength–structure relationship and increases brittleness of bone. Bone. 2011; 48:733–40. [PubMed: 21185416]
75. Rubin MR, Paschalis EP, Poundarik A, Sroga GE, McMahon DJ, et al. Advanced glycation endproducts and bone material properties in type 1 diabetic mice. PLOS ONE. 2016; 11:e0154700. [PubMed: 27140650]
76. Carriero A, Zimmermann EA, Paluszny A, Tang SY, Bale H, et al. How tough is brittle bone? Investigating osteogenesis imperfecta in mouse bone. J Bone Miner Res. 2014; 29:1392–401. [PubMed: 24420672]
77. Heveran CM, Ortega AM, Cureton A, Clark R, Livingston EW, et al. Moderate chronic kidney disease impairs bone quality in C57Bl/6J mice. Bone. 2016; 86:1–9. [PubMed: 26860048]
78. Keaveny TM, Wachtel EF, Ford CM, Hayes WC. Differences between the tensile and compressive strengths of bovine tibial trabecular bone depend on modulus. J Biomech. 1994; 27:1137–46. [PubMed: 7929463]
79. Morgan EF, Yeh OC, Chang WC, Keaveny TM. Nonlinear behavior of trabecular bone at small strains. J Biomech Eng. 2001; 123:1–9. [PubMed: 11277293]
80. Keaveny TM, Wachtel EF, Kopperdahl DL. Mechanical behavior of human trabecular bone after overloading. J Orthop Res. 1999; 17:346–53. [PubMed: 10376722]
81. Kopperdahl DL, Pearlman JL, Keaveny TM. Biomechanical consequences of an isolated overload on the human vertebral body. J Orthop Res. 2000; 18:685–90. [PubMed: 11117287]
82. Morgan EF, Keaveny TM. Dependence of yield strain of human trabecular bone on anatomic site. J Biomech. 2001; 24:569–77.
83. Hildebrand T, Laib A, Muller R, Dequeker J, Rüegsegger P. Direct three-dimensional morphomëtric analysis of human cancellous bone: microstructural data from spine, femur, iliac crest, and calcaneus. J Bone Miner Res. 1999; 14:1167–74. [PubMed: 10404017]
84. Whitehouse WJ. The quantitative morphology of anisotropic trabecular bone. J Microsc. 1974; 2:153–68.
85. Harrigan T, Mann R. Characterization of microstructural anisotropy in orthotropic materials using a second rank tensor. J Mater Sci. 1984; 19:761–67.
86. Cowin SC. The relationship between the elasticity tensor and the fabric tensor. Mech Mater. 1985; 4:137–47.

87. Banse X, Deogelaer JP, Munting E, Delloye C, Cornu O, Grynpas M. Inhomogeneity of human vertebral cancellous bone: systematic density and structure patterns inside the vertebral body. Bone. 2001; 28:563–71. [PubMed: 11344057]

88. Goldstein SA, Wilson DL, Matthews LS. The mechanical properties of human tibial trabecular bone as a function of metaphyseal location. J Biomech. 1983; 16:965–69. [PubMed: 6671987]

89. Ciarelli MJ, Goldstein SA, Kuhn JL, Cody DD, Brown MB. Evaluation of orthogonal mechanical properties and density of human trabecular bone from the major metaphyseal regions with materials testing and computed tomography. J Orthop Res. 1991; 9:674–82. [PubMed: 1870031]

90. Carter DR, Hayes WC. Bone compressive strength: the influence of density and strain rate. Science. 1976; 194:1174–76. [PubMed: 996549]

91. Morgan EF, Bayraktar HH, Keaveny TM. Trabecular bone modulus–density relationships depend on anatomic site. J Biomech. 2003; 36:897–904. [PubMed: 12757797]

92. Mosekilde L, Mosekilde LE, Danielsen CC. Biomechanical competence of vertebral trabecular bone in relation to ash density and age in normal individuals. Bone. 1987; 8:79–85. [PubMed: 3593611]

93. Odgaard A, Kabel J, van Rietbergen B, Dalstra M, Huiskes R. Fabric and elastic principal directions of cancellous bone are closely related. J Biomech. 1997; 30:487–95. [PubMed: 9109560]

94. Yang G, Kabel J, van Rietbergen B, Odgaard A, Huiskes R. The anisotropic Hooke's law for cancellous bone and wood. J Elast. 1999; 53:125–46.

95. Zysset PK, Goulet RW, Hollister SJ. A global relationship between trabecular bone morphology and homogenized elastic properties. J Biomech Eng. 1998; 120:640–46. [PubMed: 10412443]

96. Unnikrishnan GU, Gallagher JA, Hussein AI, Barest GD, Morgan EF. Elastic anisotropy of trabecular bone in the elderly human vertebra. J Biomech Eng. 2015; 137:114503. [PubMed: 26300326]

97. Chang WCW, Christensen TM, Pinilla TP, Keaveny TM. Uniaxial yield strains for bovine trabecular bone are isotropic and asymmetric. J Orthop Res. 1999; 17:582–85. [PubMed: 10459766]

98. Bevill G, Farhamand F, Keaveny TM. Heterogeneity of yield strain in low-density versus high-density human trabecular bone. J Biomech. 2009; 42:2165–70. [PubMed: 19700162]

99. Turner CH. Yield behavior of bovine cancellous bone. J Biomech Eng. 1989; 111:256–60. [PubMed: 2779192]

100. Linde F, Norgaard P, Hvid I, Odgaard A, Soballe K. Mechanical properties of trabecular bone. Dependency on strain rate. J Biomech. 1991; 24:803–9. [PubMed: 1752864]

101. Carter DR, Hayes WC. The compressive behavior of bone as a two-phase porous structure. J Bone Joint Surg. 1977; 59:954–62. [PubMed: 561786]

102. Burgers TA, Lakes RS, Garcia-Rodriguez S, Pill GR, Ploeg HL. Post-yield relaxation behavior of bovine cancellous bone. J Biomech. 2009; 42:2728–33. [PubMed: 19765712]

103. Bowman SM, Keaveny TM, Gibson LJ, Hays WC, McMahon TA. Compressive creep behavior of bovine trabecular bone. J Biomech. 1994; 27:301–5. [PubMed: 8051190]

104. Fyhrie DP, Schaffler MB. Failure mechanisms in human vertebral cancellous bone. Bone. 1994; 15:105–9. [PubMed: 8024844]

105. Nagaraja S, Couse TL, Guldberg RE. Trabecular bone microdamage and microstructural stresses under uniaxial compression. J Biomech. 2005; 38:707–16. [PubMed: 15713291]

106. Tang SY, Vashishth D. A non-invasive in vitro technique for the three-dimensional quantification of microdamage in trabecular bone. Bone. 2007; 40:1259–64. [PubMed: 17329178]

107. Goff MG, Lambers FM, Sorna RM, Keaveny TM, Hernandez CJ. Finite element models predict the location of microdamage in cancellous bone following uniaxial loading. J Biomech. 2015; 48:4142–48. [PubMed: 26522622]

108. Jungmann R, Szabo ME, Schitter G, Tang RU, Vashishth D, et al. Local strain and damage mapping in single trabeculae during three-point bending tests. J Mech Behav Biomed Mater. 2011; 4:523–34. [PubMed: 21396601]

109. Morgan EF, Yeh OC, Keaveny TM. Damage in trabecular bone at small strains. Eur J Morphol. 2005; 42:13–21. [PubMed: 16123020]
110. Lambers FM, Bouman AR, Tkachenko EV, Keaveny TM, Hernandez CJ. The effects of tensile-compressive loading mode and microarchitecture on microdamage in human vertebral cancellous bone. J Biomech. 2014; 47:3605–12. [PubMed: 25458150]
111. Arlot ME, Burt-Pichat B, Rouz JP, Vashishth D, Bouxsein ML, Delmas PD. Microarchitecture influences microdamage accumulation in human vertebral trabecular bone. J Bone Miner Res. 2008; 23:1613–18. [PubMed: 18518771]
112. Shi XT, Liu XS, Wang X, Guo XE, Niebur GL. Type and orientation of yielded trabeculae during overloading of trabecular bone along orthogonal directions. J Biomech. 2010; 43:2460–66. [PubMed: 20554282]
113. Cook RB, Zioupos P. The fracture toughness of cancellous bone. J Biomech. 2009; 42:2054–60. [PubMed: 19643417]
114. Moore TLA, Gibson LJ. Fatigue microdamage in bovine trabecular bone. J Biomech Eng. 2003; 125:769–76. [PubMed: 14986400]
115. Yamamoto E, Crawford RP, Chan DD, Keaveny TM. Development of residual strains in human vertebral trabecular bone after prolonged static and cyclic loadings at low load levels. J Biomech. 2006; 39:1812–18. [PubMed: 16038915]
116. Kosmopoulos V, Schizas C, Keller TS. Modeling the onset and propagation of trabecular bone microdamage during low-cycle fatigue. J Biomech. 2008; 41:515–22. [PubMed: 18076887]
117. Rapillard L, Charlebois M, Zysset PK. Compressive fatigue behavior of human vertebral trabecular bone. J Biomech. 2006; 39:2133–39. [PubMed: 16051256]
118. Dendorfer S, Maier HJ, Taylor D, Hammer J. Anisotropy of the fatigue behaviour of cancellous bone. J Biomech. 2008; 41:636–41. [PubMed: 18005974]
119. Cowin SC. Fabric dependence of an anisotropic strength criterion. Mech Mater. 1986; 5:251–60.
120. Pietrusczak SID, Pande GN. A fabric-dependent facture criterion for bone. J Biomech. 1999; 32:1071–79. [PubMed: 10476845]
121. Zysset PK, , Rincon-Kohli L. An alternative fabric-based yield and failure criterion for trabecular bone. In: Hozapfel GA, , Ogden RW, editorsMechanics of Biological Tissues Berlin: Springer; 2006 45770
122. Goda I, Ganghoffer JF. 3D plastic collapse and brittle fracture surface models of trabecular bone from asymptotic homogenization method. Int J Eng Sci. 2015; 87:58–82.
123. Levrero-Florencio F, Margetts L, Sales E, Xie S, Manda K, Pankaj P. Evaluating the macroscopic yield behaviour of trabecular bone using a nonlinear homogenisation approach. J Mech Behav Biomed Mater. 2016; 61:384–96. [PubMed: 27108348]
124. Garcia D, Zysset PK, Charlebois M, Curnier A. A three-dimensional elastic plastic damage constitutive law for bone tissue. Biomech Model Mechanobiol. 2009; 8:149–65. [PubMed: 18398628]
125. Charlebois M, Jirasek M, Zysset PK. A nonlocal constitutive model for trabecular bone softening in compression. Biomech Model Mechanobiol. 2010; 9:597–611. [PubMed: 20238139]
126. Gibson LJ, , Ashby MF. Cellular Solids: Structure and Properties Cambridge, UK: Cambridge Univ. Press; 1997 Cancellous bone; 42952
127. Gibson LJ. Biomechanics of cellular solids. J Biomech. 2005; 38:377–99. [PubMed: 15652536]
128. Turner CH, Cowin SC. Dependence of elastic constants of an anisotropic porous material upon porosity and fabric. J Mater Sci. 1987; 22:3178–84.
129. Zysset PK, Curnier A. An alternative model for anisotropic elasticity based on fabric tensors. Mech Mater. 1995; 21:243–50.
130. Matsuura M, Eckstein F, Lochmuller EM, Zysset PK. The role of fabric in the quasi-static compressive mechanical properties of human trabecular bone from various anatomical locations. Biomech Model Mechanobiol. 2008; 7:27–42. [PubMed: 17235622]
131. Silva MJ, Gibson LJ. The effects of non-periodic microstructure and defects on the compressive strength of two-dimensional cellular solids. Int J Mech Sci. 1997; 39:549–63.

132. van Rietbergen B, Weinans H, Huiskes R, Odgaard A. A new method to determine trabecular bone elastic properties and loading using micromechanical finite-element models. J Biomech. 1995; 28:69–81. [PubMed: 7852443]
133. Kabel J, van Rietbergen B, Odgaard A, Huiskes R. Constitutive relationships of fabric, density, and elastic properties in cancellous bone architecture. Bone. 1999; 25:481–86. [PubMed: 10511116]
134. Liu XS, Sajda P, Saha PK, Wehrli FW, Guo XE. Quantification of the roles of trabecular microarchitecture and trabecular type in determining the elastic modulus of human trabecular bone. J Bone Miner Res. 2006; 21:1608–17. [PubMed: 16995816]
135. Pauchard Y, Mattmann C, Kuhn A, Gasser JA, Boyd SK. European Society of Biomechanics S.M. Perren Award 2008: Using temporal trends of 3D bone micro-architecture to predict bone quality. J Biomech. 2008; 41:2946–53. [PubMed: 18805535]
136. Carretta R, Luisier B, Bernoulli D, Stussi E, Muller R, Lorenzetti S. Novel method to analyze post-yield mechanical properties at trabecular bone tissue level. J Mech Behav Biomed Mater. 2013; 20:6–18. [PubMed: 23455157]
137. Rho JY, Ashmann RB, Turner CH. Young's modulus of trabecular and cortical bone material: ultrasonic and microtensile measurements. J Biomech. 1993; 26:111–19. [PubMed: 8429054]
138. Turner CH, Rho J, Takano Y, Tsui TY, Pharr GM. The elastic properties of trabecular and cortical bone tissues are similar: results from two microscopic measurement techniques. J Biomech. 1999; 32:437–41. [PubMed: 10213035]
139. Lietniewski J. Determination of the elasticity coefficient for a single trabecula of a cancellous bone: scanning acoustic microscopy approach. Ultrasound Med Biol. 2005; 31:1361–66. [PubMed: 16223639]
140. Carretta R, Stussi E, Muller R, Lorenzetti S. Prediction of local ultimate strain and toughness of trabecular bone tissue by Raman material composition analysis. Biomed Res Int. 2015; 2015:457371. [PubMed: 25695083]
141. Niebur GL, Feldstein MJ, Yuen JC, Chen TJ, Keaveny TM. High-resolution finite element models with tissue strength asymmetry accurately predict failure of trabecular bone. J Biomech. 2000; 33:1575–83. [PubMed: 11006381]
142. Bayraktar HH, Morgan EF, Niebur GL, Morris GE, Wong EK, Keaveny TM. Comparison of the elastic and yield properties of human femoral trabecular and cortical bone tissue. J Biomech. 2004; 37:27–35. [PubMed: 14672565]
143. Choi K, Goldstein SA. A comparison of the fatigue behavior of human trabecular and cortical bone tissue. J Biomech. 1992; 25:1371–81. [PubMed: 1491015]
144. Torres AM, Matheny JB, Keaveny TM, Taylor D, Rimnac CM, Hernandez CJ. Material heterogeneity in cancellous bone promotes deformation recovery after mechanical failure. PNAS. 2016; 113:2892–97. [PubMed: 26929343]
145. Ding M, Odgaard A, Linde F, Hvid I. Age-related variations in the microstructure of human tibial cancellous bone. J Orthop Res. 2002; 20:615–21. [PubMed: 12038639]
146. Mosekilde L. Sex differences in age-related loss of vertebral trabecular bone mass and structure–biomechanical consequences. Bone. 1989; 10:425–32. [PubMed: 2624823]
147. McCalden RW, McGeough JA, Court-Brown CM. Age-related changed in the compressive strength of cancellous bone. The relative importance of changes in density and trabecular architecture. J Bone Joint Surg Am Ed. 1997; 79:421–27.
148. Ding M, Odgaard A, Hvid I. Changes in the three-dimensional microstructure of human tibial cancellous bone in early osteoarthritis. J Bone Joint Surg Br. 2003; 85:906–12. [PubMed: 12931817]
149. Hunter DJ, Gerstenfeld L, Bishop G, Davis AD, Mason ZD, et al. Bone marrow lesions from osteoarthritis knees are characterized by sclerotic bone that is less well mineralized. Arthritis Res Ther. 2009; 11:R11. [PubMed: 19171047]
150. Hong J, Cabe GD, Tedrow JR, Hipp JA, Snyder BD. Failure of trabecular bone with simulated lytic defects can be predicted non-invasively by structural analysis. J Orthop Res. 2004; 22:479–86. [PubMed: 15099624]

151. Hussein AI, Jackman TM, Morgan SR, Barest GD, Morgan EF. The intra-vertebral distribution of bone density: correspondence to intervertebral disc health and implications for vertebral strength. Osteoporos Int. 2013; 24:3021–30. [PubMed: 23863990]
152. Levenston ME, Beaupre GS, van der Meulen MC. Improved method for analysis of whole bonétorsion tests. J Bone Miner Res. 1994; 9:1459–65. [PubMed: 7817831]
153. Ruff CB, Hayes WC. Subperiosteal expansion and cortical remodeling of the human femur and tibia with aging. Science. 1982; 217:945–48. [PubMed: 7112107]
154. Riggs BL, Melton LJ 3rd, Robb RA, Camp JJ, Atkinson EJ, et al. Population-based study of age and sex differences in bone volumetric density, size, geometry, and structure at different skeletal sites. J Bone Miner Res. 2004; 19:1945–54. [PubMed: 15537436]
155. Keaveny TM, Kopperdahl DL, Melton LJ 3rd, Hoffmann PF, Amin S, et al. Age-dependence of femoral strength in white women and men. J Bone Miner Res. 2010; 25:994–1001. [PubMed: 19874201]
156. Rezaei A, Dragomir-Daescu D. Femoral strength changes faster with age than BMD in both women and men: a biomechanical study. J Bone Miner Res. 2015; 30:2200–6. [PubMed: 26096829]
157. Courtney AC, Wachtel EF, Myers ER, Hayes WC. Age-related reductions in the strength of the femur tested in a fall-loading configuration. J Bone Joint Surg. 1995; 77:387–95. [PubMed: 7890787]
158. Duan Y, Turner CH, Kim BT, Seeman E. Sexual dimorphism in vertebral fragility is more the result of gender differences in age-related bone gain than bone loss. J Bone Miner Res. 2001; 16:2267–75. [PubMed: 11760841]
159. Christiansen BA, Kopperdahl DL, Kiel DP, Keaveny TM, Bouxsein ML. Mechanical contributions of the cortical and trabecular compartments contribute to differences in age-related changes in vertebral body strength in men and women assessed by QCT-based finite element analysis. J Bone Miner Res. 2011; 26:974–83. [PubMed: 21542000]
160. Samelson EJ, Christiansen BA, Demissie S, Broe KE, Louie-Gao Q, et al. QCT measures of bone strength at the thoracic and lumbar spine: the Framingham study. J Bone Miner Res. 2012; 27:654–63. [PubMed: 22143959]
161. Kaptoge S, Beck TJ, Reeve J, Stone KL, Hillier TA, et al. Prediction of incident hip fracture risk by femur geometry variables measured by hip structural analysis in the study of osteoporotic fractures. J Bone Miner Res. 2008; 23:1892–904. [PubMed: 18684092]
162. Bouxsein ML, Karasik D. Bone geometry and skeletal fragility. Curr Osteoporos Rep. 2006; 4:49–56. [PubMed: 16822403]
163. Roux JP, Wegrzyn J, Arlot ME, Guyen O, Delmas PD, et al. Contribution of trabecular and cortical components to biomechanical behavior of human vertebrae: an ex vivo study. J Bone Miner Res. 2010; 25:356–61. [PubMed: 19653808]
164. Nekkanty S, Yerramshetty J, Kim DG, Zauel R, Johnson E, et al. Stiffness of the endplate boundary layer and endplate surface topography are associated with brittleness of human whole vertebral bodies. Bone. 2010; 47:783–89. [PubMed: 20633709]
165. Heilmeier U, Cheng K, Pasco C, Parrish R, Nirody J, et al. Cortical bone laminar analysis reveals increased midcortical and periosteal porosity in type 2 diabetic postmenopausal women with history of fragility fractures compared to fracture-free diabetics. Osteoporos Int. 2016; 27:2791–802. [PubMed: 27154435]
166. Osima M, Kral R, Borgen TT, Hogestol IK, Joakimsen RM, et al. Women with type 2 diabetes mellitus have lower cortical porosity of the proximal femoral shaft using low-resolution CT than nondiabetic women, and increasing glucose is associated with reduced cortical porosity. Bone. 2017; 97:252–60. [PubMed: 28161589]
167. Nilsson AG, Sundh D, Johansson L, Nilsson M, Mellstrom D, et al. Type 2 diabetes mellitus is associated with better bone microarchitecture but lower bone material strength and poorer physical function in elderly women: a population-based study. J Bone Miner Res. 2017; 32:1062–71. [PubMed: 27943408]
168. Reilly DT, Burstein AH. The elastic and ultimate properties of compact bone tissue. J Biomech. 1975; 8:393–96. [PubMed: 1206042]

169. Mirzaali MJ, Schwiedrzik JJ, Thaiwichai S, Best JP, Michler J, et al. Mechanical properties of cortical bone and their relationships with age, gender, composition and microindentation properties in the elderly. Bone. 2016; 93:196–211. [PubMed: 26656135]

170. Dong XN, Acuna RL, Luo Q, Wang X. Orientation dependence of progressive post-yield behavior of human cortical bone in compression. J Biomech. 2012; 45:2829–34. [PubMed: 22995144]

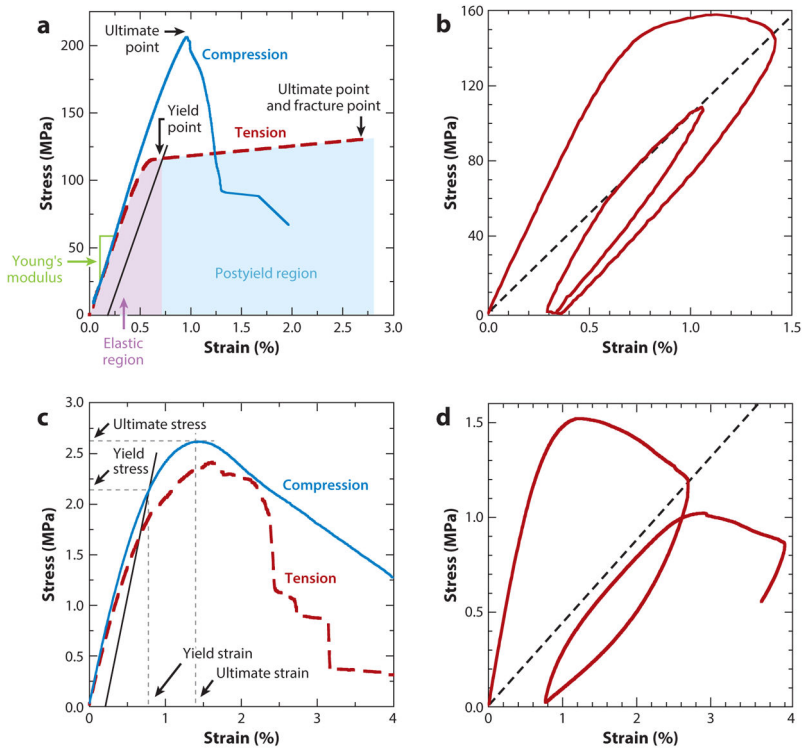

Figure 1.

Stress–strain curves for (*a*,*b*) cortical bone tested along the longitudinal direction and (*c*,*d*) trabecular bone tested along the principal direction. Panels *a* and *c* show monotonic tests in tension and compression, and panels *b* and *d* show load–unload–reload tests. Panels *a* and *c* are annotated with some basic material properties. The dashed lines in panels *b* and *d* indicate the perfect damage modulus, which is the secant modulus at the point at which the initial loading ramp is reversed to begin the unloading. Both types of bone tissue exhibit a reloading modulus that is initially equal to the original Young's modulus but then decreases to equal the perfect damage modulus. Modified from References 3 and 80 with permission.

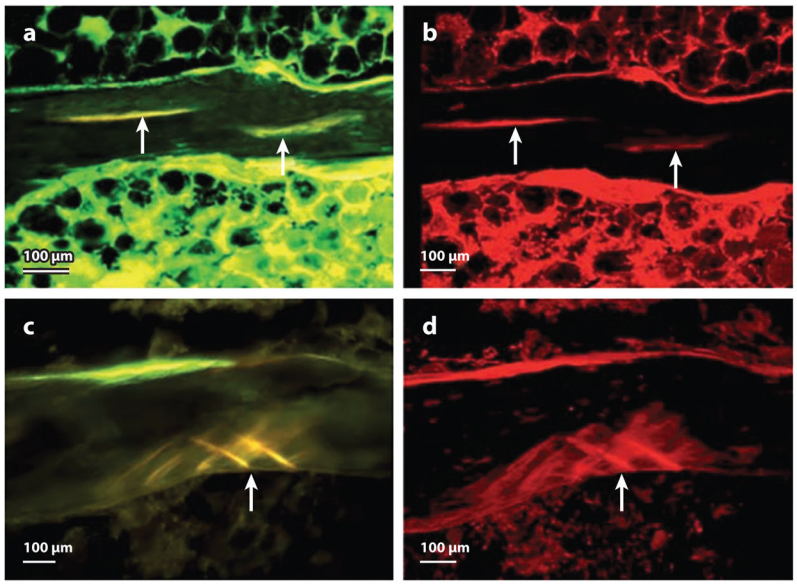

Figure 2.
Microdamage in human vertebrae. (*a*,*b*) Linear microcrack. (*c*,*d*) Diffuse damage. Panels *a* and *c* were acquired using bright-field microscopy; panels *b* and *d* were acquired using laser scanning confocal microscopy (stain is xylenol orange). Modified from Reference 111 with permission.

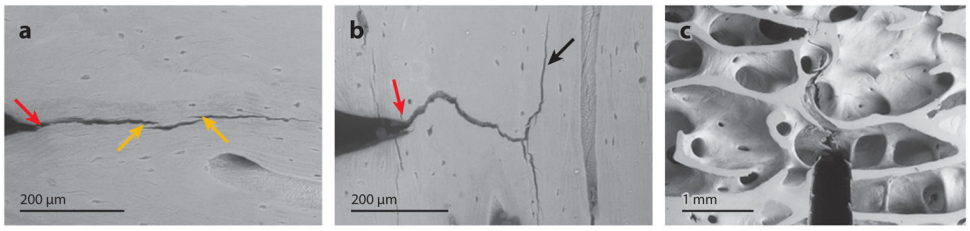

Figure 3.

(*a*,*b*) Crack propagation emanating from a notch (*red arrow*) in cortical bone. (*c*) Crack propagation in trabecular bone. Toughening mechanisms in cortical bone include uncracked ligament bridging (*yellow arrows*) and crack deflection (*black arrow*). Modified from References 19 and 113 with permission.

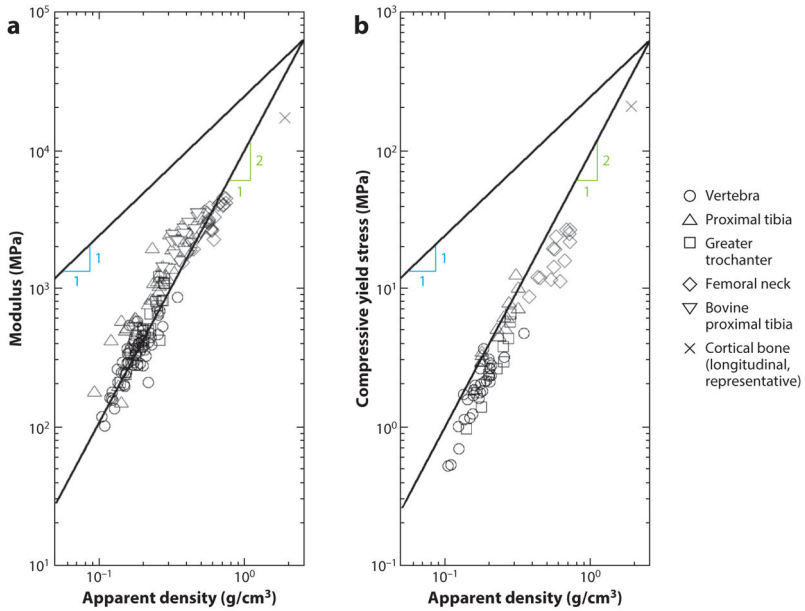

Figure 4.

Log–log plots for (*a*) Young's modulus and (*b*) compressive yield strength as functions of apparent density. Lines indicating power-law exponents of one and two are drawn on the plots. Modified from References 82 and 91 with permission.

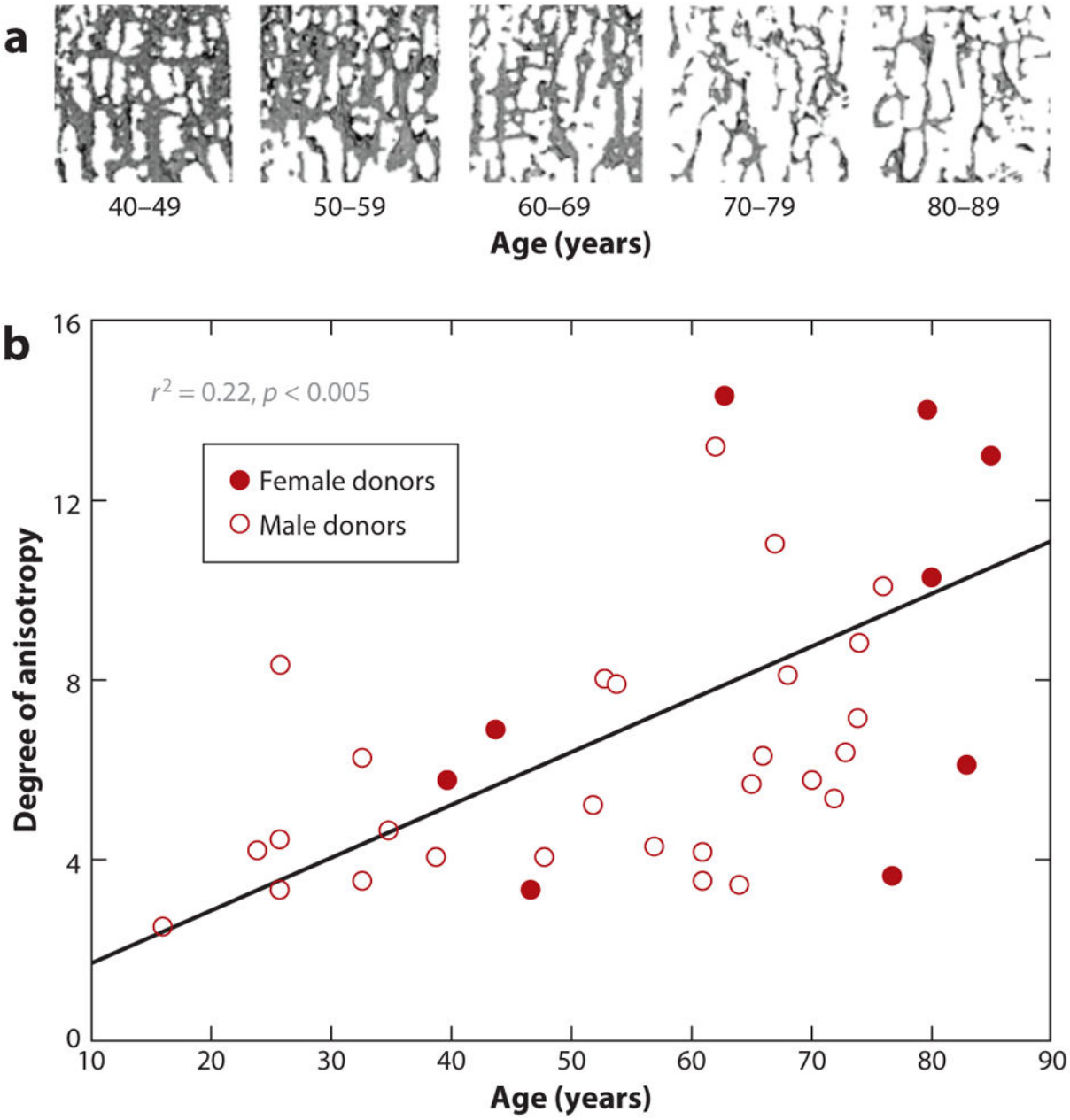

Figure 5.

Increase in anisotropy with age. (*a*) Representative cross sections of cylindrical specimens from the trabecular compartment of the human proximal tibia from donors in the age ranges indicated below each rendering. (*b*) Degree of anisotropy plotted against donor age. Modified from Reference 145 with permission.

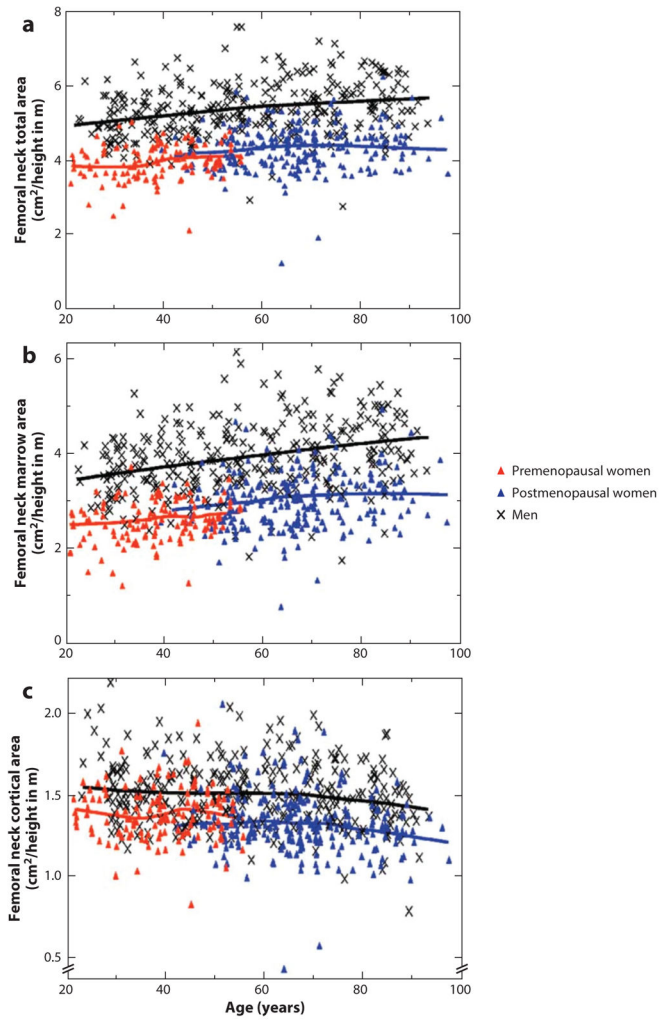

Figure 6.

(*a*) Total cross-sectional area, (*b*) marrow cross-sectional area, and (*c*) cortical cross-sectional area in the human femoral neck, all plotted as a function of age. Red, blue, and black symbols indicate premenopausal women, postmenopausal women, and men, respectively. Modified from Reference 154 with permission.

Table 1

Elastic, yield, and ultimate properties of human femoral cortical bone[a]

Longitudinal direction	
Elastic modulus (MPa)	17,900 ± 3,900[b] 18,160 ± 1,880[c]
Poisson's ratio	0.62 ± 0.26[b]
Tensile yield stress (MPa)	71.56 ± 10.19[c,f]
Tensile yield strain (%)	0.67 ± 0.04[c,f]
Tensile ultimate stress (MPa)	135 ± 15.6[b] 92.95 ± 10.07[c]
Tensile ultimate strain (%)	1.9 ± 0.6[c]
Compressive yield stress (MPa)	115.06 ± 16.36[c,f]
Compressive yield strain (%)	0.98 ± 0.09[c,f]
Compressive ultimate stress (MPa)	205 ± 17.3[b] 153.59 ± 21.63[c]
Compressive ultimate strain (%)	1.3 ± 0.3[c]
Shear modulus (MPa)	3,300 ± 400[c] 6,070 ± 570[c]
Shear yield stress (MPa)	40.95 ± 5.16[c,f]
Shear yield strain (%)	0.87 ± 0.04[c,f]
Shear ultimate stress (MPa)	65 ± 4.0[b] 46.31 ± 5.82[c]
Transverse direction	
Elastic modulus (MPa)	10,100 ± 2,400[b] 5,650 ± 1,610[d] 6,490 ± 3,220[e]
Poisson's ratio	0.62 ± 0.26[b]
Tensile ultimate stress (MPa)	53 ± 10.7[b]
Compressive yield stress (MPa)	41.8 ± 19.4[d] 44.1 ± 21.1[e]
Compressive yield strain (%)	0.83 ± 0.42[d] 0.84 ± 0.23[e]
Compressive ultimate stress (MPa)	131 ± 20.7[b] 65.2 ± 13.8[d] 63.1 ± 20.7[e]

[a]The values listed were obtained from mechanical tests performed on specimens with characteristic dimensions on the order of 1 cm.

[b]From Reference 168.

[c]From Reference 169.

[d]Circumferential direction (170).

[e] Radial direction (170).

[f] Calculated using 0.2% offset.